Atmospheric
Measurement
Techniques
Discussions

Characteristics of aerosol vertical profiles in Tsukuba, Japan, and their impacts on the evolution of the atmospheric boundary layer

Rei Kudo[1], Toshinori Aoyagi[2], and Tomoaki Nishizawa[3]

[1]Meteorological Research Institute, Japan Meteorological Agency, Tsukuba, 305-0052, Japan
5   [2]Japan Meteorological Agency, Tokyo, 100-8122, Japan
[3]National Institute for Environmental Studies, Tsukuba, 305-0053, Japan

Correspondence to: Rei Kudo (reikudo@mri-jma.go.jp)

Abstract. Vertical profiles of the aerosol physical and optical properties, with a focus on seasonal means and on transport
10   events, were investigated in Tsukuba, Japan, by a synergistic remote sensing method that uses lidar and sky radiometer data.
The retrieved aerosol vertical profiles were input into our developed one-dimensional atmospheric model, and the impacts of
the aerosol vertical profiles on the evolution of the atmospheric boundary layer (ABL) were studied by numerical sensitivity
experiments. The retrieval results in the spring showed that aerosol optical thickness was greater in the free atmosphere (FA)
than in the ABL owing to the frequent occurrence of transported aerosols in the FA. In other seasons, optical thickness in the
15   FA was almost the same as that in the ABL. The aerosol optical and physical properties in the ABL showed a dependency on
the extinction coefficient, whereas large variability in the physical and optical properties of aerosols in the FA were
attributed to transport events, during which the transported aerosols consisted of varying amounts of dust and smoke
particles depending on where they originated (China, Mongolia, or Russia). Numerical sensitivity experiments based on
simulations conducted with and without aerosols showed that aerosols caused the net downward radiation and the sensible
20   and latent heat fluxes at the surface to decrease. Direct heating of aerosols in the FA strengthened the capping inversion
around the top of the ABL. Consequently, the ABL height was decreased in simulations with aerosols compared with
simulations without aerosols. We also conducted simulations in which all aerosols were compressed into the ABL but in
which the columnar properties were the same and compared with the simulation results for uncompressed aerosol profiles.
The results showed that the reductions in net downward radiation and in sensible and latent heat fluxes were the same in both
25   types of simulations, but in the simulations with compression the capping inversion was weakened owing to aerosol direct
heating in the ABL, and as a result the ABL height was increased compared with that in the simulations without compression.
These results suggest that the vertical profile of aerosol direct heating has important effects on the ABL evolution.

Atmospheric
Measurement
Techniques
Discussions

1 Introduction

Solar radiation heats the Earth's surface, thereby causing thermal instability and evaporation. The thermal energy and water vapor are transported into the atmosphere through turbulent mixing in the atmospheric boundary layer (ABL). These processes in the ABL have important implications for global energy and water circulation. Aerosols have significant impacts

5   on the radiation budget of the Earth because they scatter and absorb solar radiation (aerosol–radiation interaction) and modify cloud physical properties (aerosol–cloud interaction) (IPCC, 2013). In this study, we focus on aerosol–radiation interaction and did not consider clouds and precipitation processes. Direct scattering and absorption of solar radiation by aerosols decrease the amount of solar radiation that reaches the Earth's surface and sensible and latent heat fluxes, heat the atmosphere, and modify atmospheric stability. These effects have significant impacts on the evolution of the ABL, but the

10 impacts differ depending on the aerosol optical properties (Yu et al., 2002; Pandithurai et al., 2008).

Yu et al. (2002) and Pandithurai, et al. (2008) investigated the influences of aerosol optical properties on the ABL structure by sensitivity experiments with a high resolution ABL model coupled with an accurate radiative transfer model. They showed that the light absorption characteristics of aerosols are important determinates of their impact on ABL evolution. However, these studies focused on aerosols only in the ABL. Tsunematsu et al. (2006) examined sounding data

15 obtained by frequently launched sondes and showed that direct heating of transported dust in the free atmosphere (FA) strengthened the capping inversion at the top of the ABL. Therefore, it is also necessary to study the influences of aerosols in the FA on ABL evolution, especially because aerosols in the FA can be transported both regionally and globally (Uno et al., 2009).

Ground-based remote sensing has the advantage that it can be used for continuous monitoring of aerosol vertical

20 profiles. We developed a synergistic method, SKYLIDAR, that retrieves vertical profiles of aerosol optical properties from lidar and sun/sky photometer data (Kudo et al., 2016). SKYLIDAR provides vertical profiles of the extinction coefficient, single-scattering albedo, and phase function, and with these products the solar heating rate can be evaluated (Kudo et al., 2016). Then, by inputting the retrieved aerosol optical properties into an ABL model, it is possible to investigate the influences of aerosols in the ABL and FA on the evolution of the ABL.

25 In this study, we first evaluated the characteristics of the vertical profiles of aerosol physical and optical properties in a two-year lidar and sun/sky photometer data set collected at Tsukuba, Japan, in a rural area located near the mega-city of Tokyo. The columnar properties of aerosols at Tsukuba have been investigated by many researchers (e.g., Nishizawa et al., 2004; Kudo et al., 2010a, 2010b, 2011), but these previous studies did not investigate their vertical profiles statistically. Second, we investigated the impact of aerosol vertical profiles on the evolution of the ABL by conducting numerical

30 sensitivity experiments with our developed one-dimensional (1-D) atmospheric model. Details of the data set and methodologies are described in Sect. 2. The characteristics of the aerosol vertical profiles and results of the sensitivity experiments conducted with the 1-D atmospheric model are presented in Sect. 3. Our findings are summarized in Sect. 4.

2 Data and methodology

2.1 Remote sensing of aerosol vertical profiles

2.1.1 Data retrieval

The vertical profiles of aerosol optical and physical properties were estimated from sky radiometer and lidar data obtained by
5   the SKYLIDAR remote sensing method (Kudo et al., 2016). The sky radiometer (Prede Co., Ltd, Tokyo, Japan), deployed in
the SKYNET (Takamura and Nakajima, 2004), is a scanning photometer that measures direct solar radiation and the angular
distribution of diffuse radiation. In this study, we used observation data at the Meteorological Research Institute (MRI) of
Japan Meteorological Agency (JMA) in Tsukuba (36.05°N, 140.12°E). The wavelengths of the sky radiometer data are 340,
380, 400, 500, 675, 870, and 1020 nm. We also used data from a two-wavelength Mie scattering lidar deployed by AD-Net
10 (Sugimoto et al., 2015) at the National Institute for Environmental Studies (NIES) near MRI. The lidar data consisted of the
attenuated backscatter coefficients for particle and molecular scattering at 532 and 1064 nm, and the depolarization ratio for
particle and molecular scattering at 532 nm. The sky radiometer and lidar observation data were collected during 2012 and
2013. As auxiliary data, we used vertical profiles of pressure and temperature from the U.S. National Centers for
Environmental Prediction (NCEP) 6-hourly reanalysis data set (Kalnay et al., 1996), total ozone from observations made at
15 the JMA Aerological Observatory (AO) near MRI, and surface albedo from the 5-year climatology of the Filled Land
Surface Albedo Product, which was generated from the official Terra/MODIS-derived Land Surface Albedo Product
(Moody et al., 2005, 2007; Moody 2008). The MRI, NIES and AO instruments are all located within a circle with a radius of
1 km.

SKYLIDAR estimates aerosol vertical profiles by the following two steps, based on a maximum a posteriori
20 scheme (Kudo et al., 2016). In the first step, the columnar values of the aerosol physical and optical properties (optical
thickness, single-scattering albedo, etc.) are estimated by optimizing real and imaginary parts of the refractive index, volume
size distribution, and volume ratio of non-spherical particles in the coarse mode to all of the sky radiometer data and the
vertical mean of the depolarization ratio of the lidar data. Volume size distribution is assumed to follow a bi-modal
lognormal distribution, and the volumes, mode radii, and widths of the fine and coarse modes are estimated. The optical
25 properties of non-spherical particles are calculated from a data table of randomly oriented spheroids (Dubovik et al., 2006).
In the second step, the vertical profiles of the volume concentrations of fine and coarse modes, the volume ratio of non-
spherical particles in the coarse mode, and the real and imaginary parts of the refractive index are optimized to all of the lidar
data and to the optical thickness and single-scattering albedo obtained in the first step. The final outputs are vertical profiles
of the extinction coefficient, single-scattering albedo, phase function, the real and imaginary parts of the refractive index, the
30 bi-modal volume size distribution, and the volume ratio of non-spherical particles in the coarse mode. The output
wavelengths of the optical properties are 532 and 1064 nm. Note that the mode radii and width of the fine and coarse modes
in the second step are fixed by the columnar values obtained in the first step. These outputs enable us to use the radiative
transfer model to calculate the vertical profile of the solar heating rate (Kudo et al., 2016).

2.1.2 Determination of ABL height

Locally emitted aerosols in the ABL and the transported aerosols in the FA can have different optical properties, which can be evaluated separately after the ABL height has been determined. We estimated the ABL height from the lidar data by the method of Baars et al. (2008), which is based on the wavelet covariance transform (WCT) with the Haar function. The WCT

5 method is less affected by signal noise than the gradient and variance methods. The local maximum of the WCT vertical profile corresponds to the ABL height, and the local minimum corresponds to the base height of clouds or of transported aerosols. In this study, the ABL height was determined by the following procedure:

(1) The attenuated backscatter coefficients at 532 and 1064 nm were normalized by its maximum value below 1000 m, and the WCTs for data at 532 and 1064 nm were calculated.

10 (2) The local minima and maxima of the WCT vertical profiles at 532 and 1064 nm were detected.

(3) The base height of clouds (or transported aerosols) was searched by using a threshold of –0.1 for the local minimum of the WCT at 532 nm.

(4) If the base height was not detected in step (3), it was repeated using the WCT at 1064 nm. If the base height was still not detected, it was considered absent or unclear.

15 (5) The ABL height was searched by using a threshold of 0.05 for the local maximum of the WCT at 532 nm in the day-time, and of the WCT at 1064 nm at night. The top height of the search range was below the base height, if the base height of clouds or transported aerosols was detected in steps (3) or (4).

(6) If the ABL height was not detected, the threshold in step (5) was decreased by –0.01, and the search was repeated until the threshold reached to 0.01.

20 (7) If the ABL height was not detected in step (6), the search was repeated using the WCT at another wavelength.

(8) If the ABL height was not detected in step (7), the ABL height was considered undetermined.

(9) The time series of ABL height was smoothed by the running–mean.

Figure 1 shows the examples of the determined ABL height together with the extinction coefficient estimated by SKYLIDAR. The ABL height could be determined very well when transported aerosols were well above the ABL (Fig 1a).

25 However, when transported aerosols become mixed with the aerosols in the ABL, the ABL height could not be detected (see from 0 to 7 UTC 2 April in Fig. 1b). In this case, we considered aerosols below base height to be in the ABL and those above to be in the FA.

2.2 Model simulation

2.2.1 1-D atmospheric model

30 We developed a 1-D atmospheric model, consisting of ABL and radiative transfer (RT) schemes, and conducted sensitivity experiments to investigate the radiative impact of aerosols on the evolution of the ABL. The ABL scheme in the model is based on the ABL model used as the JMA operational mesoscale model for weather forecasting in Japan. The RT scheme is

an RT model developed in our laboratory for the remote sensing of aerosols and clouds and their impacts on the radiative balance in the solar and infrared wavelength regions (Asano and Shiobara, 1989; Nishizawa et al., 2004; Kudo et al., 2011).

The 1-D atmospheric model has a high resolution atmospheric vertical grid with 70 layers from the surface to 40 km. The thickness of the bottom layer is 5 m. Turbulent mixing is calculated by the Mellow-Yamada-Nakanishi-Niino Level 3 scheme (Nakanishi, 2001; Nakanishi and Niino, 2004, 2006), and calculations of surface fluxes are based on the Monin-Obukhov similarity using the universal function of Beljaars and Holtslag (1991). The vertical grid in the soil has 10 layers from the surface to 2 m depth, and the soil temperature is calculated by solving the diffusion equation. The water content in the soil layers was fixed in this study.

In the 1-D atmospheric model, vertical diffusion terms for turbulent mixing and vertical advection by a prescribed vertical motion field are considered for the vertical mixing of potential temperature, specific humidity and the horizontal component of wind. Neither cloud formation nor precipitation is included. In addition, vertical diffusion of aerosols is not considered in the model; aerosol vertical profiles are fixed by the initially given ones.

In the RT scheme, the solar spectrum from 300 nm to 3.0 μm and the infrared spectrum from 4. 0 to 50.0 μm are divided into 54 and 19 intervals, respectively. The downward and upward fluxes and the heating rate are calculated by the doubling and adding method (Lacis and Hansen, 1974). Gaseous absorption of water vapor, carbon dioxide, oxygen, and ozone are calculated by the correlated k-distribution method. Scattering at the ground surface is assumed to be Lambert reflection.

The aerosol parameters input to the RT scheme are the vertical profiles of the extinction coefficient, single-scattering albedo, and the phase function at wavelengths from 300 nm to 3.0 μm. However, because the wavelengths of the SKYLIDAR retrievals are limited to 532 and 1064 nm, we determined the optical properties between 532 and 1064 nm by linear interpolation and used the optical properties at 532 and 1064 nm for wavelengths of less than 532 nm and greater than 1064 nm, respectively (Kudo et al., 2016). The influences of aerosols on the infrared wavelength region are ignored.

2.2.2 Sensitivity experiments

We conducted three types of simulation experiments to investigate the impact of aerosols on the evolution of the ABL. The first type was simulations without aerosols (EXP0), the second was simulations using the observed aerosol vertical profile (EXP1), and the third was the same as the second one but with the entire aerosol vertical profile was compressed into the bottom 1 km (EXP2). Note that the columnar optical properties in EXP1 and EXP2 simulations were the same; only the vertical profile differed between them. Thus, the influences of aerosols can be evaluated from the difference between EXP0 and EXP1 simulations, and the influences of the aerosol vertical profile can be investigated by comparing the results of EXP2 and EXP1 simulations. We conducted experiments using the springtime mean of the aerosol vertical profile and the aerosol vertical profiles observed in the spring during five aerosol transport events in the FA.

To set up the model parameter, we referred to the sensitivity experiments conducted by Yu et al. (2002) and Pandithurai et al. (2008). For our sensitivity experiments, we used the following specified parameters in the 1-D atmospheric

model. The integration time of all simulations was 24 hours with a time step of 1 minute. The solar orientation was set to that on 5 April 2012 at 36.05°N. The surface albedo was set to the spring mean of the 5-year climatology of the Filled Land Surface Albedo Product (Moody et al., 2005, 2007; Moody 2008). The vertical motion was set to the spring mean of NCEP 6-hourly reanalysis data set. The initial vertical profiles of pressure, temperature, specific humidity, and horizontal wind

5   were also set to the spring means of the NCEP 6-hourly reanalysis data set. The soil surface was assumed to be bare, and the heat capacity and thermal conductivity in the soil layers were set to 1.3×10^6 J m^{-3} K^{-1} and 0.3 W m^{-1} K^{-1}, respectively, based on values for dry sandy clay (Kondo, 1994). The initial temperatures in the soil layers were based on the spring mean of the soil temperature observed at the weather observation field of Mito Meteorological Observatory (Ministry of Agriculture, Forestry, and Fisheries, and Japan Meteorological Agency, 1982), which is 60 km north of the MRI.

10   Because the sensible and latent heat fluxes at the surface depend on the water content of the soil, we performed sensitivity experiments for both dry and wet soils. The daily means of the sensible and latent heat fluxes in EXP0 for the dry soil case (volumetric water content 0.1) were 88 and 78 W m^{-2}, respectively. For the wet soil case (volumetric water content 0.2), the sensible heat flux was decreased by 22 W m^{-2}, and the latent heat flux was increased by 32 W m^{-2}. These differences affected the ABL structures (e.g., temperature and specific humidity) in the EXP1 and EXP2 experiments, but

15   not the impacts of aerosols (i.e., the signs of differences, EXP1 – EXP0 or EXP2 – EXP0 were either both positive or both negative in the dry and wet soil cases, and their absolute values were not significantly different). Therefore, we do not show the results for the wet soil case in this paper. Thus, the volumetric water content in the soil layers was fixed at 0.1.

3 Results

3.1 Characteristics of aerosol vertical profiles

20   **3.1.1 Seasonal characteristics**

Frequency distributions of the extinction coefficient at 532 nm, based on daily means, were obtained for spring (43 analyzed days), summer (7 days), autumn (35 days), and winter (59 days) (Fig. 2). In all the seasons, the extinction coefficient was large in three layers: from the surface to 1.5 km; from 1.5 to 3.5 km; and from 3.5 to 6 km altitude. The bottom layer is the ABL, and the aerosols in this layer originate primarily from local emissions. The two upper layers are in the FA, and most

25   aerosols in these layers have been transported long distances. Transported aerosols are frequently observed in the FA in spring, autumn, and winter, when low-pressure systems carrying aerosols emitted in the eastern region of the Eurasian continent frequently pass over Japan. In summer, Japan is dominated by a high-pressure system, so it receives fewer transported aerosols. In our data, the optical thickness in summer, autumn, and winter were almost the same in the ABL and FA, but in spring, optical thickness was larger in the FA than in the ABL (Table 1).

30   In general, the ABL height is high in summer and low in winter, but in our results, the ABL height was higher in winter and spring, and lower in summer and autumn (Fig. 2). The higher ABL heights in winter and spring can be attributed

to the mixing of aerosols between the ABL and FA, which makes it difficult to determine the ABL height (see Sect. 2.1.2). The low ABL height in summer and autumn may be influenced by clouds, which form near the top of the convective mixed layer. Under these circumstances, the ABL height cannot be determined from only lidar data.

5 The Ångström exponent is a parameter related to particle size: a smaller value indicates a larger particle size. The Ångström exponent in the ABL increased as the extinction coefficient increased (Fig. 3). This result suggests that large extinction coefficients were mainly due to small particles, such as sulfate, nitrate, and organics. Conversely, background aerosols consist of large particles, such as locally emitted mineral dust, likely derived from the large areas of bare soil exposed by agriculture and urban development in Tsukuba. The Ångström exponent in the middle and top layers ranged from 0.0 to 2.5. This large variability can be attributed to differences in the composition of aerosols, in particular, the

10 proportions of dust and smoke particles, during transport events. The characteristics of five transport events are described in Sect. 3.1.2.

Single-scattering albedo is an important parameter related to light absorption. In the FA, single-scattering albedo was around 0.95 with small variability (Fig. 4 and Table 1), but in the ABL, it decreased as the extinction coefficient decreased. In general, the single-scattering albedo of dust particles is small, whereas that of small particles, other than black

15 carbon, is large. The dependency of the single-scattering albedo on the extinction coefficient in the ABL is therefore consistent with the particle size result shown in Fig. 3.

The asymmetry factor is an indicator of how much solar energy reaches the surface: a large asymmetry factor value indicates strong forward scattering, which means that more solar energy reaches to surface. In addition, the value of the asymmetry factor is inversely proportional to that of the Ångström exponent. In our results, large variation of the asymmetry

20 factor was observed in the FA, and a dependency of the asymmetry factor on the extinction coefficient was observed in the ABL (Fig. 5).

The values of other important optical and physical parameters are shown in Table 1. These values are particularly useful for comparisons of aerosols in different areas. The values of the real and imaginary parts of the refractive index were almost same values in both the ABL and FA and in all the seasons. Similarly, the values of the mode radius and width

25 mostly did not differ among seasons, although the coarse mode radius was smaller in spring. The smaller coarse mode radius in spring reflects the relatively small coarse mode radius of the transported aerosols, which ranged from 1.93 to 3.61 μm (Table 2). In each season, the volume ratio of non-spherical particles in the coarse mode in the ABL was larger than that in the FA, owing to the presence of local dust in the ABL; the smallest value in the ABL was observed in summer, when the ground surface is generally covered with grasses and few dust particles are emitted from the surface. The lidar ratio

30 (extinction to backscatter ratio) is an important parameter for estimating the extinction coefficient, particularly when only the lidar data are available for that purpose. In our results, no clear seasonal difference was observed in the lidar ratio.

3.1.2 Aerosol transport events in the FA

The optical thickness in the FA was largest in spring among all seasons because of presence of transported aerosols. From our results obtained over two years, we selected for further examination five events, which occurred on 2 April 2012 and 16 April and 8, 9, and 14 May 2013, characterized by large optical thickness in the FA. The daily means of the optical and physical properties of transported aerosols in the FA on these five dates are summarized in Fig. 6 and Table 2. Large extinction coefficients were observed in the top and middle layers (see Sect. 3.1.1) during these five transport events (Fig. 6a). In addition, we inferred that the aerosols during the events on 2 April 2012, 16 April and 14 May 2013 consisted primarily of transported dust, because on these dates the volume of coarse-mode particles was particularly large (Fig. 6b), Ångström exponent values were small, and the volume ratio of non-spherical particles was large (Table 2). The two-day backward trajectories for those events (Fig. 6c) suggest that the transported dust originated in desert areas of China and Mongolia. On 8 May 2013, the volume of fine-mode particles was very large (Fig. 6b), the Ångström exponent was also large, and the volume ratio of non-spherical particles was small (Table 2); these results indicate that the aerosols consisted dominantly of small and spherical particles. The backward trajectory (Fig. 6c) indicated that the source region was in Russia, to the southeast area of Lake Baikal, where a forest fire had been observed in early May 2013. Therefore, we interpreted this transported aerosol to consist of transported smoke particles were from that forest fire. The following day, 9 May 2013, the source had moved to northeastern China (Fig. 6c), and the volume of coarse-mode particles was large (Fig. 6b); these results suggest that this aerosol may have consisted of transported smoke and dust particles. The values of the Ångström exponent and the volume ratio of non-spherical particles in the coarse mode tended to differ between transported dust and smoke events, but the other physical and optical properties did not show clear differences between different types of events (Table 2).

3.2 Sensitivity experiment results

3.2.1 Impact of aerosols on the evolution of the ABL

Figure 7 and Table 3 show the results of EXP0 and EXP1 – EXP0. The net downward surface radiation in the solar and infrared wavelength regions, as well as the sensible and latent heat fluxes, were decreased in the EXP1 simulations (with aerosols) compared with EXP0 simulation (without aerosols) (Figs. 7a–c). The change in the daily mean ranged from -14 to -23 W m^{-2} for the net downward radiation, from -7 to -11 W m^{-2} for the sensible heat flux, and from -6 to -10 W m^{-2} for the latent heat flux (Table 3). Absorption by the ground was also decreased; the change in the daily ranged from -1.3 to -2.2 Wm^{-2} (Table 3). In general, the downward surface solar radiation becomes small when optical thickness is large, single-scattering albedo is small, and the asymmetry factor is small, (Kudo et al., 2010b). The single-scattering albedo and asymmetry factor were not very different between the springtime mean and the five transport events (Tables 1 and 2), so the reduction of the net downward radiation (Fig. 7a) mainly reflects the optical thickness of the column (Table 3), and the reductions of the sensible and latent heat fluxes were caused by the decrease of the net downward radiation. The potential

Atmospheric
Measurement
Techniques
Discussions

temperature profile at noon local time decreased in the ABL owing to the decline in the sensible heat flux (Fig. 7d). Note that in the 1-D atmospheric model results, the latent heat flux could not warm the atmosphere in the ABL because condensation is not included in the model. The daily maximum 2 m temperature was decreased by 0.2 to 0.6 K (Table 3). In contrast, the potential temperature increased in the FA owing to the direct heating of transported aerosols. The vertical profiles of direct

5 heating depended on the profiles of the extinction coefficient (Fig. 6a). The warming of the FA and the cooling of the ABL stabilized the atmosphere and strengthened the capping inversion around the top of the ABL. The strengthened capping inversion and the decline of the sensible heat flux caused the ABL height to decease by -133 to -208 m (Fig. 7f and Table 3).

The latent heat flux, that is, the water vapor flux, was apparently decreased by aerosols, but the change in the amount of surface evaporation was small, from -0.21 to -0.36 kg m^{-2} day^{-1} (Fig. 7c and Table 3). The change in the vertical

10 profile of specific humidity was very small, but the specific humidity around the top of the ABL was decreased as a result of the decrease in the ABL height and the dry air in the FA (Fig. 7e).

3.2.2 Impact of the aerosol vertical profile on the evolution of the ABL

Figure 8 and Table 3 show the results of EXT0 and EXP2 – EXP0. Note that the entire aerosol vertical profile was compressed in the bottom 1 km in the EXP2 simulations, but the optical thickness of the column was the same as that in the

15 EXP1 simulations. The influence of only the aerosol vertical profile can thus be investigated by comparing Figs. 7 and 8. The amounts of decrease in the net downward radiation and the sensible and latent heat fluxes in the EXP2 simulations were almost the same as those in the EXP1 simulations (Figs. 8a-c). However, the decrease in the potential temperature in the ABL was smaller in EXP2 than in EXP1 (Fig. 8d), because aerosol direct heating in the ABL was stronger in EXP2 than in EXP1. The changes in surface evaporation (Table 3) and specific humidity (Fig. 8e) in EXP2 were similar to those in EXP1.

20 Since aerosol direct heating in the ABL, together with the lack of direct heating in the FA, weakened the capping inversion around the top of the ABL, the decrease in the ABL height was smaller in EXP2 than in EXP1. Thus, the evolution of the ABL was changed by the aerosol vertical profile, even though the columnar characteristics of the aerosol optical properties were the same. The impacts of aerosols on the ABL structure, that is, reductions of the temperature in the ABL and of the ABL height, were larger when aerosols were present in the FA.

25 ### 4 Conclusion

We investigated vertical profiles of aerosol physical and optical properties at Tsukuba, Japan, with focus on the seasonal means and on five aerosol transport events, by a synergistic remote sensing method (SKYLIDAR) using sky radiometer and lidar data in two years (2012 and 2013). In addition, we investigated the impact of the aerosol vertical profile on the evolution of the ABL by conducting sensitivity experiments with our 1-D atmospheric model.

30 The vertical profiles of the seasonal mean extinction coefficients showed three distinct aerosol layers, the ABL, and two layers in the FA. In spring, the optical thickness in the FA was larger than that in the ABL, whereas in other seasons, the

optical thickness was almost the same in the ABL and FA. The physical and optical properties of the aerosols in the ABL were dependent on the extinction coefficient: As the extinction coefficient increased, the Ångström exponent and single-scattering albedo increased and the asymmetry factor decreased. The large extinction coefficient in the ABL was attributed to an increase of the small particles.

5 The optical and physical properties in the FA varied greatly owing to the presence of transported aerosols. We investigated the vertical profiles and backward trajectories of five transport events. In three events, the aerosol consisted of dust particles transported from desert regions of China and Mongolia. In one event, the aerosol consisted of small smoke particles transported from a forest fire in Russia. The aerosols of a fifth event consisted of both small and large particles which we interpreted as smoke and dust particles, respectively. The parameters dependent on particle size (Ångström exponent and asymmetry factor) were consistent with these interpretations, whereas other parameters such as single-scattering albedo did not differ much among the five events.

 We conducted sensitivity experiments in which the spring mean aerosol vertical profile and the aerosol vertical profiles of the five transport events were input into our 1-D atmospheric model. The sensitivity experiments with (EXP1) and without aerosols (EXP0) showed that the aerosols decreased net downward surface radiation and sensible and latent heat fluxes. Furthermore, direct heating of the transported aerosols in the FA strengthened the capping inversion near the top of the ABL. Consequently, the ABL height was less developed in EXP1 simulations than in the EXP0 simulations. To investigate the impact of only the aerosol vertical profile on the evolution of the ABL, we conducted simulations (EXP2) in which all aerosols were compressed into the ABL (0-1 km altitude), but in which the columnar optical thickness was the same as that in the EXP1 simulations. The net downward radiation and the sensible and latent heat fluxes were not changed, but the ABL height was increased, in EXP2 simulations compared with EXP1 simulations. This increase in the ABL height resulted from a weakened capping inversion caused by aerosol direct heating in the ABL and the lack of direct heating in the FA. The sensitivity experiment results suggest that the vertical profile of aerosol direct heating is an essential factor in the evolution of the ABL. Moreover, it is particularly important to characterize aerosol optical properties in the FA because aerosols in the FA can be transported widely and therefore affect the ABL both regionally and globally.

 Our 1-D atmospheric model did not consider cloud formation or precipitation, although both of these can be affected by aerosol-induced modification of atmospheric stability. In the future, we plan to develop a 1-D or 3-D model that includes these processes and investigate aerosol-cloud interactions by inputting the observed aerosol data into the models.

Atmospheric
Measurement
Techniques
Discussions

5 Data availability

The lidar data are available from the AD-Net (http://www-lidar.nies.go.jp). The sky radiometer data are available from the SKYNET (http://www-lidar.nies/go/jp/skynet/), but the sky radiometer data at Tsukuba, Japan are available on request by contacting the first author of the paper.

5

Atmospheric
Measurement
Techniques
Discussions

References

Asano, S. and Shiobara, M.: Aircraft measurements of the radiative effects of tropospheric aerosols: I. Observational Results of the Radiation Budget, J. Meteorol. Soc. Japan, 847–861, 1989.

Baars, H., Ansmann, A., Engelmann, R. and Althausen, D.: Continuous monitoring of the boundary-layer top with lidar, Atmos. Chem. Phys., 8, 7281–7296, doi:10.5194/acpd-8-10749-2008, 2008.

Beljaars, A. C. M., Holtslag, A. A. M.: Flux Parameterization over Land Surfaces for Atmospheric Models, J. Appl. Meteorol., 30, 327–341, 1991.

Dubovik, O., Sinyuk, A., Lapyonok, T., Holben, B. N., Mishchenko, M., Yang, P., Eck, T. F., Volten, H., Muñoz, O., Veihelmann, B., van der Zande, W. J., Leon, J. F., Sorokin, M. and Slutsker, I.: Application of spheroid models to account for aerosol particle nonsphericity in remote sensing of desert dust, J. Geophys. Res. Atmos., 111(11), 1–34, doi:10.1029/2005JD006619, 2006.

IPCC: Climate Change 2013: The Physical Science Basis. Contribution of Working Group I to the Fifth Assessment Report of the Intergovernmental Panel on Climate Change [Stocker, T.F., D. Qin, G.-K. Plattner, M. Tignor, S.K. Allen, J. Boschung, A. Nauels, Y. Xia, Cambridge University Press, Cambridge, United Kingdom and New York, NY, USA., 2013.

Kalnay, E., Kanamitsu, M., Kistler, R., Collins, W., Deaven, D., Gandin, L., Iredell, M., Saha, S., White, G., Woollen, J., Zhu, Y., Chelliah, M., Ebisuzaki, W., Higgins, W., Janowiak, J., Mo, K. C., Ropelewski, C., Wang, J., Leetmaa, A., Reynolds, R., Jenne, R., and Joseph, D.: The NCEP/NCAR 40-Year Reanalysis Project, Bull. Am. Meteorol. Soc., 437–471, 1996.

Kondo, J.: Mizukankyo-no-kisyougaku (in Japanese), 2nd editio., Asakura Publishing Co. Ltd., Tokyo., 1994.

Kudo, R., Uchiyama, A., Yamazaki, A., Sakami, T. and Kobayashi, E.: From solar radiation measurements to optical properties: 1998-2008 trends in Japan, Geophys. Res. Lett., 37(4), 1–6, doi:10.1029/2009GL041794, 2010a.

Kudo, R., Uchiyama, A., Yamazaki, A. and Kobayashi, E.: Seasonal characteristics of aerosol radiative effect estimated from ground-based solar radiation measurements in Tsukuba, Japan, J. Geophys. Res. Atmos., 115(1), 1–10, doi:10.1029/2009JD012487, 2010b.

Kudo, R., Uchiyama, A., Yamazaki, A., Sakami, T. and Ijima, O.: Decadal changes in aerosol optical thickness and single scattering albedo estimated from ground-based broadband radiometers: A case study in Japan, J. Geophys. Res. Atmos., 116(3), 1–14, doi:10.1029/2010JD014911, 2011.

Kudo, R., Nishizawa, T. and Aoyagi, T.: Vertical profiles of aerosol optical properties and the solar heating rate estimated by combining sky radiometer and lidar measurements, Atmos. Meas. Tech., 9(7), 3223–3243, doi:10.5194/amt-9-3223-2016, 2016.

Lacis, A., A., Hansen, J. E.: A Parameterization for the Absorption of Solar Radiation in the Earth's Atmosphere, , 31, 118–133, 1974.

LP DAAC: Land Processes Distributed Active Archive Center: The Land Cover Type Climate Modeling Grid (CMG)
product (MCD12C1). Version 051. NASA EOSDIS Land Processes DAAC, USGS Earth Resources Observation and
Science (EROS) Center, Sioux Falls, South Dakota, [online] Available from:
https://lpdaac.usgs.gov/dataset_discovery/modis/modis_products_table/mcd12c1 (Accessed 20 May 2007), 2013.

5 Ministry of Agriculture, Forestry, and Fisheries, and J. M. A.: Chichu-ondo-nado-ni-kansuru-shiryou [Report about the soil
temperature] (in Japanese), Tokyo., 1982.

Moody, E. G.: MODIS-derived spatially complete surface albedo products: Spatial and temporal pixel and zonal averages, J.
Appl. Meteorol. Climatol., 47(11), 2879–2894, doi:10.1175/2008JAMC1795.1, 2008.

Moody, E. G., King, M. D., Platnick, S., Schaaf, C. B. and Gao, F.: Spatially complete global spectral surface albedos:

10 Value-added datasets derived from terra MODIS land products, IEEE Trans. Geosci. Remote Sens., 43(1), 144–157,
doi:10.1109/TGRS.2004.838359, 2005.

Moody, E. G., King, M. D., Schaaf, C. B., Hall, D. K. and Platnick, S.: Northern Hemisphere five-year average (2000-2004)
spectral albedos of surfaces in the presence of snow: Statistics computed from Terra MODIS land products, Remote Sens.
Environ., 111(2), 337–345, doi:10.1016/j.rse.2007.03.026, 2007.

15 Nakanishi, M.: Closure Model Based on Large-Eddy Simulation Data, , 349–378, 2001.

Nakanishi, M. and Niino, H.: An improved Mellor-Yamada Level-3 model with condensation physics: Its design and
verification, Boundary-Layer Meteorol., 112(1), 1–31, doi:10.1023/B:BOUN.0000020164.04146.98, 2004.

Nakanishi, M. and Niino, H.: An improved Mellor-Yamada Level-3 model: Its numerical stability and application to a
regional prediction of advection fog, Boundary-Layer Meteorol., 119(2), 397–407, doi:10.1007/s10546-005-9030-8,

20 2006.

NEO: NASA Earth Observatory: The imagery of MODIS active fire, [online] Available from: http://neo.sci.gsfc.nasa.gov/
(Accessed 16 July 2016), 2016.

Nishizawa, T., Asano, S., Uchiyama, A. and Yamazaki, A.: Seasonal variation of aerosol direct radiative forcing and optical
properties estimated from ground based radiative measurements, J. Atmos. Sci., 61, 57–72, 2004.

25 Pandithurai, G., Seethala, C., Murthy, B. S. and Devara, P. C. S.: Investigation of atmospheric boundary layer characteristics
for different aerosol absorptions: Case studies using CAPS model, Atmos. Environ., 42(19), 4755–4768,
doi:10.1016/j.atmosenv.2008.01.038, 2008.

Sugimoto, N., Nishizawa, T., Shimizu, A., Matsui, I., Jin, Y., Higurashi, A., Uno, I., Hara, Y., Yumimoto, K. and Kudo, R.:
Continuous observations of atmospheric aerosols across East Asia, SPIE Newsroom, 2–5, doi:10.1117/2.1201510.006178,

30 2015.

Takamura, T. and Nakajima, T.: Overview of SKYNET and its activities, Opt. Pura Apl, 37(3), 3303–3308, 2004.

Tsunematsu, N., Sakai, T. and Nagai, T.: Strong capping inversion over the Tokyo metropolitan area associated with
airborne Asian dust, Geophys. Res. Lett., 33(19), 1–5, doi:10.1029/2006GL026645, 2006.

13

Uno, I., Eguchi, K., Yumimoto, K., Takemura, T., Shimizu, A., Uematsu, M., Liu, Z., Wang, Z., Hara, Y. and Sugimoto, N.:
Asian dust transported one full circuit around the globe, Nat. Geosci., 2(8), 557–560, doi:10.1038/ngeo583, 2009.

Yu, H., Liu, S. C. and Dickinson, R. E.: Radiative effects of aerosols on the evolution of the atmospheric boundary layer, J.
Geophys. Res., 107, doi:10.1029/2001JD000754, 2002.

5

14

Atmospheric
Measurement
Techniques
Discussions

Table 1. Seasonal means and standard deviations (in parentheses) of aerosol optical and physical properties

Physical and optical properties		Spring		Summer		Autumn		Winter	
		ABL	FA	ABL	FA	ABL	FA	ABL	FA
Optical thickness at 532 nm		0.08	0.13	0.07	0.07	0.05	0.05	0.05	0.06
		(0.03)	(0.08)	(0.02)	(0.05)	(0.02)	(0.02)	(0.02)	(0.04)
Ångströme exponent		0.81	0.97	0.84	1.53	1.18	1.05	1.06	1.11
		(0.36)	(0.52)	(0.46)	(0.17)	(0.35)	(0.26)	(0.40)	(0.38)
Single scattering albedo at 523 nm		0.93	0.96	0.92	0.92	0.96	0.95	0.96	0.96
		(0.03)	(0.01)	(0.05)	(0.06)	(0.03)	(0.03)	(0.02)	(0.03)
Asymmetry factor at 532 nm		0.70	0.68	0.71	0.66	0.66	0.67	0.66	0.66
		(0.03)	(0.03)	(0.04)	(0.04)	(0.03)	(0.03)	(0.04)	(0.04)
Real part of refractive index at 532 nm		1.44	1.46	1.41	1.41	1.42	1.41	1.42	1.42
		(0.05)	(0.04)	(0.03)	(0.02)	(0.04)	(0.03)	(0.05)	(0.03)
Imaginary part of refractive index at 532 nm		0.006	0.003	0.006	0.008	0.003	0.003	0.002	0.002
		(0.004)	(0.002)	(0.004)	(0.006)	(0.002)	(0.002)	(0.002)	(0.002)
Mode radius (µm)	fine	0.14 (0.02)		0.14 (0.04)		0.12 (0.03)		0.11 (0.02)	
	coarse	2.83 (1.45)		4.59 (1.37)		4.70 (2.00)		5.89 (2.30)	
Mode width	fine	0.46 (0.13)		0.59 (0.09)		0.53 (0.13)		0.60 (0.13)	
	coarse	0.92 (0.10)		0.98 (0.02)		0.98 (0.02)		0.97 (0.06)	
Volume ratio of non-spherical particles in the coarse mode		0.96	0.85	0.79	0.68	0.95	0.91	0.97	0.86
		(0.06)	(0.22)	(0.20)	(0.21)	(0.08)	(0.09)	(0.07)	(0.14)
Lidar ratio at 532 nm		69 (10)	58 (7)	68 (23)	65 (13)	57 (10)	63 (10)	56 (9)	56 (10)

Table 2. Daily means of optical and physical properties of transported aerosols in the FA

Physical and optical properties		2 April 2012	16 April 2013	8 May 2013	9 May 2013	14 May 2013
Optical thickness at 532 nm		0.33	0.24	0.27	0.33	0.25
Ångströme exponent		0.49	0.47	1.82	1.28	0.78
Single-scattering albedo at 532 nm		0.98	0.97	0.97	0.96	0.95
Asymmetry factor at 532 nm		0.68	0.71	0.64	0.65	0.68
Real part of the refractive index at 532 nm		1.53	1.43	1.42	1.53	1.48
Imaginary part of the refractive index at 532 nm		0.001	0.001	0.003	0.004	0.004
Mode radius (µm)	fine	0.15	0.13	0.14	0.15	0.15
	coarse	2.43	2.28	2.15	3.61	1.93
Mode width	fine	0.31	0.46	0.43	0.44	0.48
	coarse	0.90	0.89	0.98	0.98	0.77
Volume ratio of non-spherical particles in the coarse mode		0.99	0.97	0.34	0.96	0.84
Lidar ratio at 532 nm		47	56	61	55	56

Atmospheric
Measurement
Techniques
Open Access
EGU

Discussions

Table 3: Results of EXP0, EXP1, and EXP2 sensitivity experiments

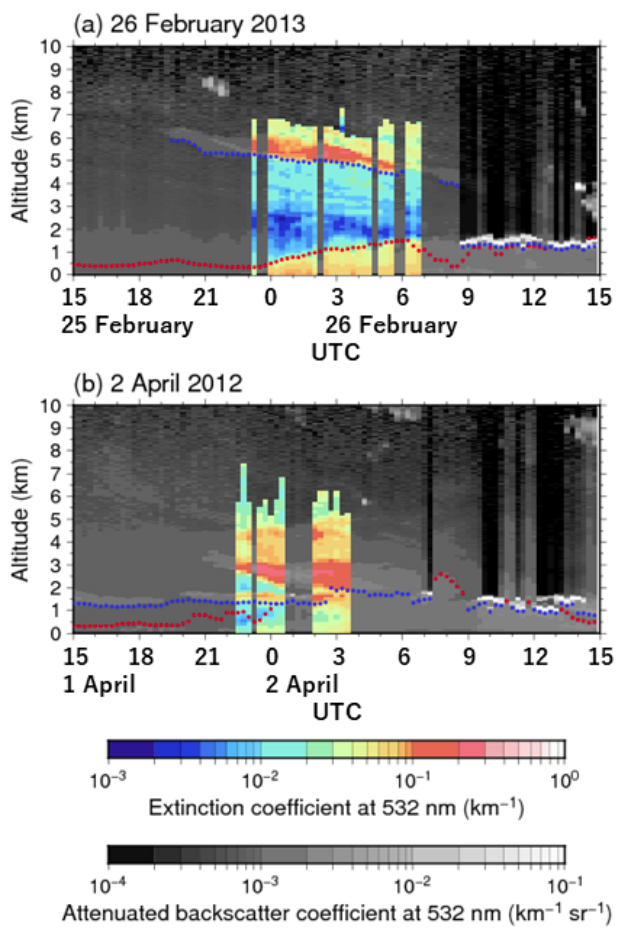|	Aerosol optical thickness in the column (532 nm)	Daily mean net downward radiation (W m⁻²)	Daily mean sensible heat flux (W m⁻²)	Daily mean latent heat flux (W m⁻²)	Daily mean ground absorption (W m⁻²)	Daily mean of 2 m temperature (K)	Daily maximum of 2 m temperature (K)	Daily integrated surface evaporation (kg m⁻² day⁻¹)	Daily maximum ABL height (m)
EXP0									
Spring mean	0.0	166	88	78	-0.6	285	293	2.68	2352
EXP1 – EXP0									
Spring mean	0.21	-14	-7	-6	-1.3	-0.3	-0.2	-0.21	-133
2 Apr 2012	0.38	-22	-10	-10	-2.2	-0.5	-0.6	-0.34	-186
16 Apr 2013	0.35	-19	-9	-8	-1.8	-0.4	-0.4	-0.29	-162
8 May 2013	0.32	-18	-8	-8	-1.7	-0.4	-0.4	-0.27	-150
9 May 2013	0.42	-23	-11	-10	-2.2	-0.5	-0.5	-0.36	-208
14 May 2013	0.37	-22	-11	-10	-2.1	-0.5	-0.5	-0.33	-163
EXP2 – EXP0									
Spring mean	0.21	-14	-7	-5	-1.2	-0.2	-0.1	-0.18	-24
2 Apr 2012	0.38	-22	-11	-9	-1.9	-0.4	-0.2	-0.30	-72
16 Apr 2013	0.35	-19	-9	-8	-1.7	-0.3	-0.2	-0.26	-83
8 May 2013	0.32	-18	-9	-7	-1.6	-0.3	-0.2	-0.25	-77
9 May 2013	0.42	-23	-12	-9	-2.0	-0.4	-0.3	-0.32	-90
14 May 2013	0.37	-22	-11	-9	-1.9	-0.3	-0.2	-0.30	-70

Figure 1. Two examples showing the determined ABL height (red dots) and the base height of clouds or transported aerosols (blue dots).
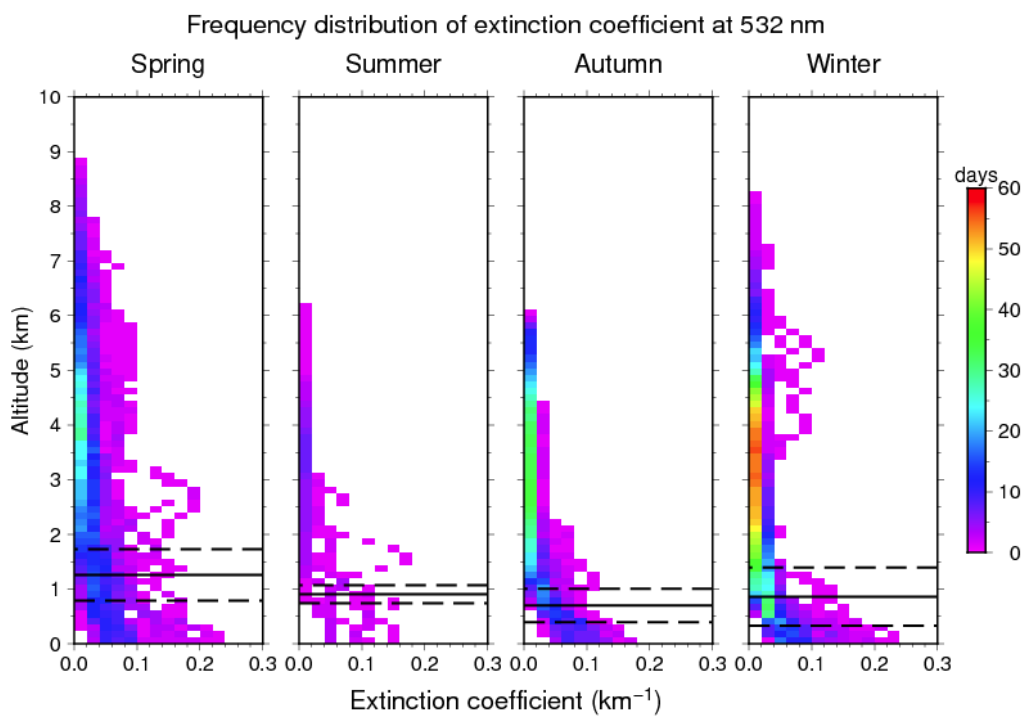
Figure 2. Frequency distributions of the extinction coefficient at 532 nm by seasons. The solid horizonal and dashed lines indicate the seasonal means and standard deviations of the ABL height.
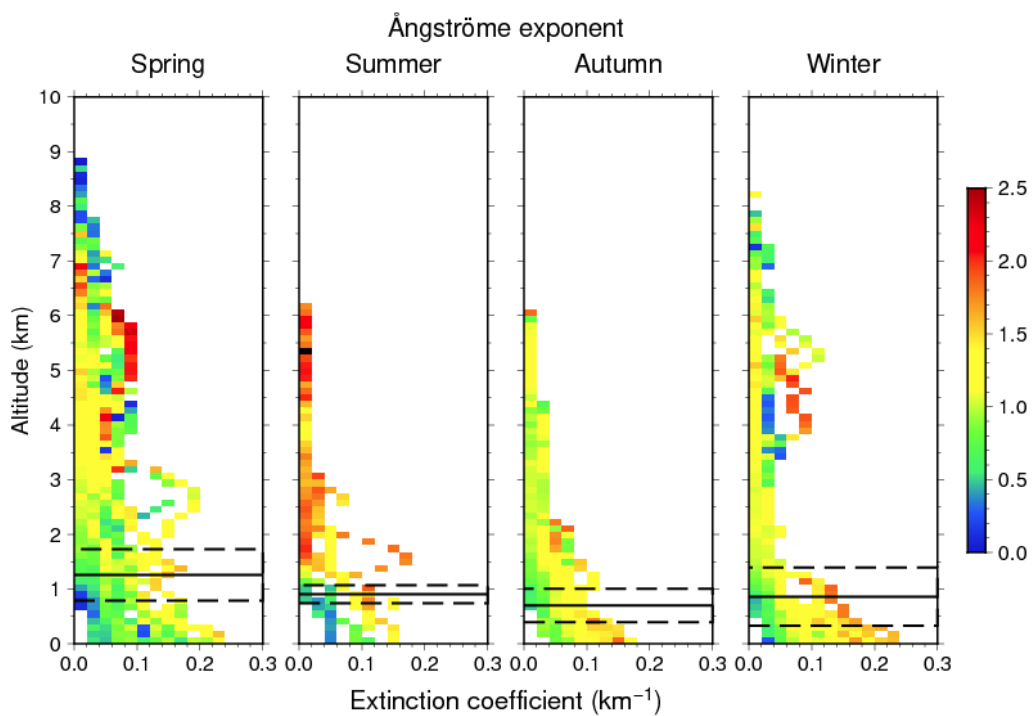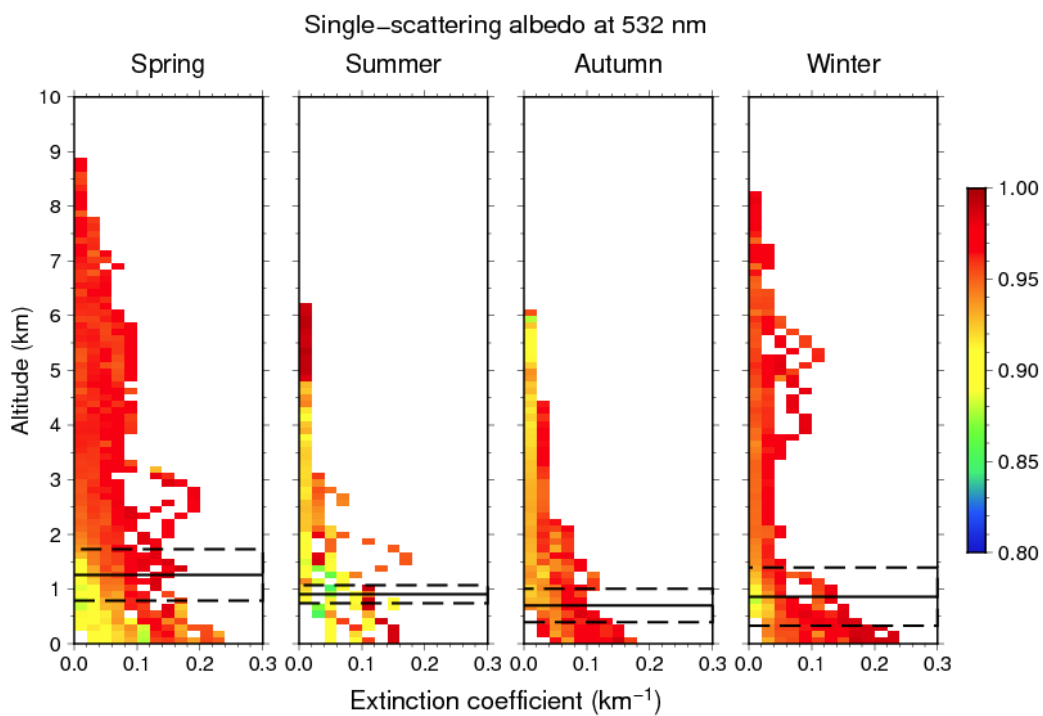
5

Atmospheric
Measurement
Techniques
Open Access
Discussions
EGU

Figure 3. Dependencies of the Ångström exponent on the extinction coefficient at 532 nm and the altitude by seasons. The solid and dashed lines indicate the seasonal means and standard deviations of the ABL height.
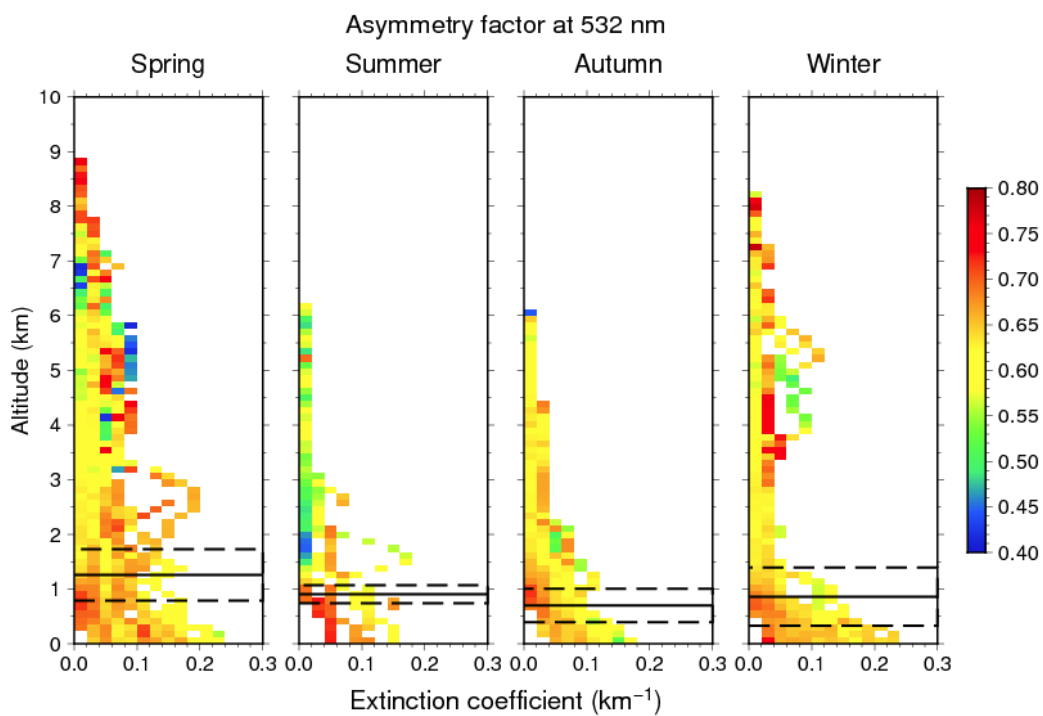
Atmospheric
Measurement
Techniques
Discussions

Figure 4. Dependencies of single-scattering albedo on the extinction coefficient at 532 nm and the altitude by seasons. The solid and dashed lines indicate the seasonal means and standard deviations of the ABL height.
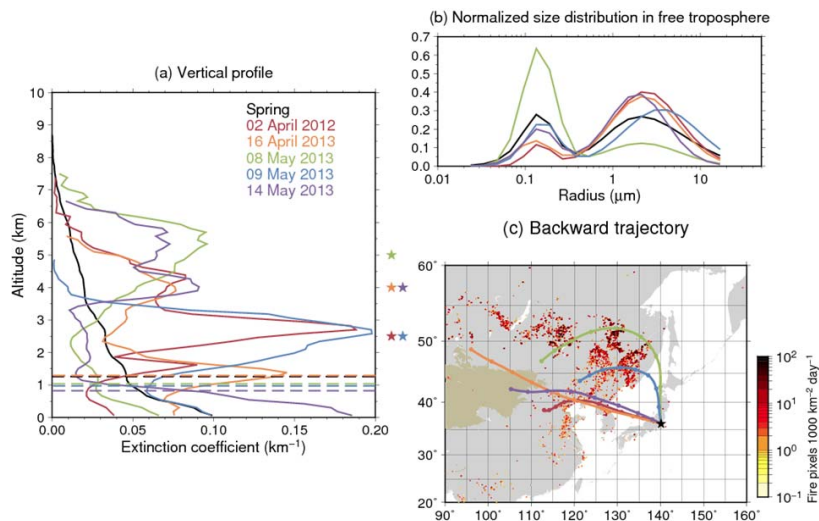
Figure 5. Dependencies of asymmetry factor on the extinction coefficient at 532 nm and the altitude by season. The solid and dashed lines indicate the seasonal means and standard deviations of the ABL height.

Figure 6. Optical and physical properties of transported aerosols in the FA: (a) vertical profile of the extinction coefficient at 532 nm with the ABL height (dashed lines), (b) normalized size distribution over the FA, and (c) 2-day backward trajectory. The stars in (a) indicate the start altitude of the backward trajectories shown in (c). The color scale in (c) indicates fire activity from 1 to 9 May 2013, based on MODIS active-fire product data (NEO, 2016). The ochre color indicates desert regions, based on data of the Land Cover Type Climate Modeling Grid product (LP DAAC, 2013).
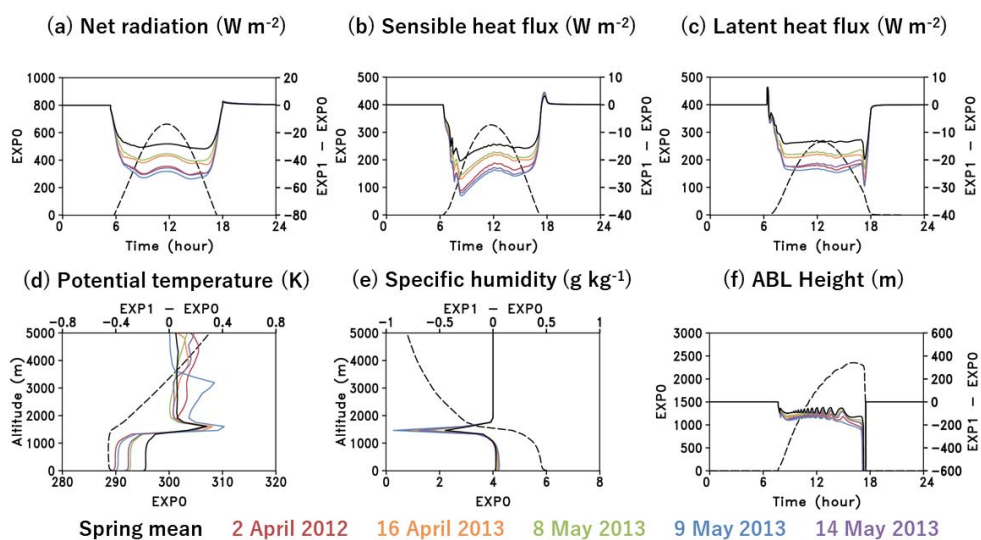
Figure 7. Results of EXP0 (dashed line) and the difference between EXP1 and EXP0 (solid lines): (a) net downward surface radiation, (b) sensible heat flux, (c) latent heat flux, (d) potential temperature at 12:00 LST, (e) specific humidity at 12:00 LST, and (f) ABL height.
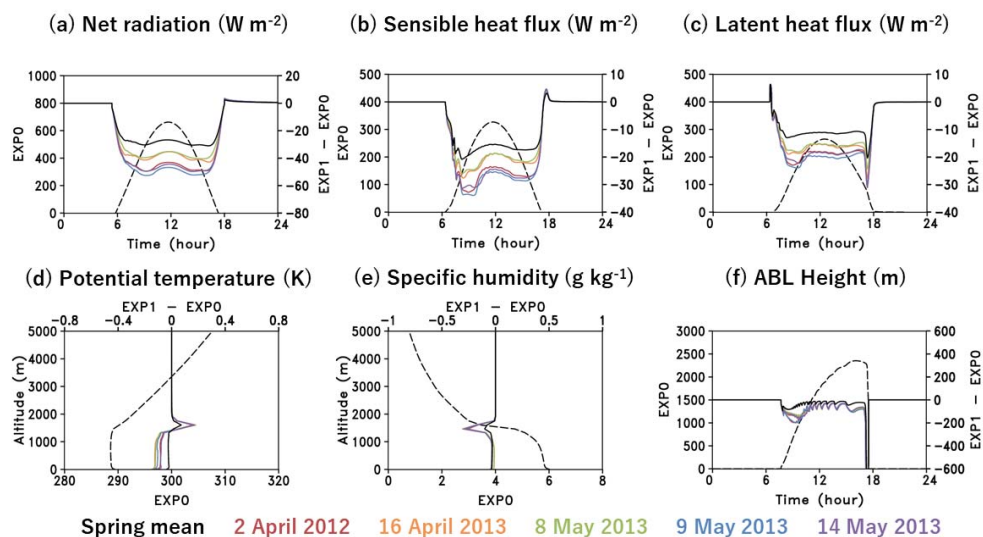
5

Figure 8. Results of EXP0 (dashed line) and the difference between EXP2 and EXP0 (solid lines): (a) net radiation at the surface, (b) sensible heat flux, (c) latent heat flux, (d) potential temperature at 12:00 LST, (e) specific humidity at 12:00 LST, and (f) ABL height.